Clinical Cancer Research

Noninvasive Measurement of mTORC1 Signaling with ^{89}Zr-Transferrin

Charles Truillet[1], John T. Cunningham[2], Matthew F.L. Parker[1], Loc T. Huynh[1], Crystal S. Conn[2,3], Davide Ruggero[2,3], Jason S. Lewis[4,5], and Michael J. Evans[1,3]

Abstract

Purpose: mTOR regulates many normal physiological processes and when hyperactive can drive numerous cancers and human diseases. However, it is very challenging to detect and quantify mTOR signaling noninvasively in clinically relevant animal models of disease or man. We hypothesized that a nuclear imaging tool measuring intracellular mTOR activity could address this unmet need.

Experimental Design: Although the biochemical activity of mTOR is not directly amenable to nuclear imaging probe development, we show that the transferrin receptor can be used to indirectly measure intracellular changes in mTOR activity.

Results: After verifying that the uptake of radiolabeled transferrin (the soluble ligand of the transferrin receptor) is stimulated by active mTORC1 *in vitro*, we showed that ^{89}Zr-labeled transferrin (Tf) can measure mTORC1 signaling dynamics in normal and cancerous mouse tissues with PET. Finally, we show that ^{89}Zr-Tf can detect the upregulation of mTORC1 by tumor cells to escape the antitumor effects of a standard-of-care antiandrogen, which is to our knowledge the first example of applying PET to interrogate the biology of treatment resistant cancer.

Conclusions: In summary, we have developed the first quantitative assay to provide a comprehensive measurement of mTOR signaling dynamics *in vivo*, in specific normal tissues, and during tumor development in genetically engineered animal models using a nuclear imaging tool that is readily translatable to man. *Clin Cancer Res; 23(12); 3045–52. ©2016 AACR.*

Introduction

The serine/threonine kinase mTOR is a master regulator of cellular growth, metabolism, and survival (1). In normal tissues, distinct environmental inputs like growth factors and amino acids conditionally activate mTOR, which in turn translates these stimuli to control gene expression at the transcription and translation levels. Because of its widespread importance to cellular physiology, dysregulation leading to hyperactivation of mTOR activity is implicated in numerous cancers and benign human diseases. In these contexts, biochemical inhibitors of mTOR like the natural product rapamycin as well as ATP-site inhibitors have shown preclinical and, in some cases, clinical activities.

The mixed clinical success of mTOR inhibitors underscores the more general observation that it is currently very challenging to identify cells harboring hyperactive mTOR in higher organisms. The gold standard approach to interrogate mTOR signaling—probing mTOR phosphosubstrate levels with immunoblot or immunohistochemistry—requires tissue, and biopsy for research purposes is challenging to justify and execute in humans. Tissue access is not a problem for animal models; however, acquiring tissue often necessitates euthanizing the subject, which precludes careful longitudinal analysis of mTOR signaling dynamics. Finally, biopsy by nature provides only a narrow view of the biology within the sampled tissue, a concern for the accurate characterization of molecularly heterogeneous diseases and complex signaling between distant normal organs. These considerations led us to hypothesize that a noninvasive biomarker that measures mTOR activity could substantially increase our understanding of mTOR biology in complex higher organisms.

Although the kinase activity of mTOR is not obviously amenable to radiotracer development, we proposed that an "imageable" protein regulated by mTOR could indirectly measure its activity (2). Because cancer cells require the cofactor Fe^{3+} to support cellular proliferation, we hypothesized that mTOR may impact the biology of transferrin (Tf), the serum ligand responsible for chaperoning circulating Fe^{3+} into eukaryotic cells. Indeed, it is known that mTORC1 can activate the transcription factors HIF1α and MYC, either of which have been shown to stimulate transcription of the transferrin receptor (TFRC) in model systems (3, 4).

Material and Methods

General methods

HEK293, T47D, HCT-15, U87 MG, U138 MG, U251, U373 MG, and PC3 were acquired from ATCC and subcultured

[1]Department of Radiology and Biomedical Imaging, University of California San Francisco, San Francisco, California. [2]Department of Urology, University of California San Francisco, San Francisco, California. [3]Helen Diller Family Comprehensive Cancer Center, University of California San Francisco, San Francisco, California. [4]Department of Radiology and the Molecular Pharmacology Program, Memorial Sloan Kettering Cancer Center, New York. [5]Departments of Radiology and Pharmacology, Weill Cornell Medical College, New York.

Note: Supplementary data for this article are available at Clinical Cancer Research Online (http://clincancerres.aacrjournals.org/).

Current address for J.T. Cunningham: Department of Cancer Biology, University of Cincinnati College of Medicine, 3125 Eden Avenue, Cincinnati, OH 45267.

Corresponding Authors: Michael J. Evans, Department of Radiology and Biomedical Imaging, University of California San Francisco, 185 Berry St., Lobby 6, Suite 350, San Francisco, CA 94107. Phone: 415-353-3442; Fax: 415-353-4925; E-mail: michael.evans@ucsf.edu; and Jason S. Lewis, Memorial Sloan Kettering Cancer Center, 1275 York Avenue, New York, NY 10065. Phone: 646-888-3038; E-mail: lewisj2@mskcc.org

doi: 10.1158/1078-0432.CCR-16-2448

Translational Relevance

Molecular imaging tools that directly measure intracellular oncogene activity could significantly impact the diagnosis and monitoring of tumor biology posttherapy. Our data with ^{89}Zr-transferrin is translationally relevant because of the importance of mTORC1 to numerous cancers and human disease, and we recently completed IND enabling studies to begin human imaging with this radiotracer.

according to manufacturer's recommendations. LNCaP-AR was a generous gift from Dr. Charles Sawyers at MSKCC (New York, NY). PrEC LHS cells were a gift from Dr. Phil Febbo. RAD001, BEZ235, INK128, and doxorubicin were purchased from Selleckchem and solubilized with DMSO for *in vitro* studies. Human holo-transferrin was purchased from Sigma-Aldrich and succinimidyl-DFO was obtained from Macrocyclics. Zirconium-89 was purchased from 3D Imaging, LLC. Iodine-125 was purchased from Perkin Elmer.

Animal studies

All animal studies were conducted in compliance with the Institutional Animal Care and Use Committee at UCSF. ^{89}Zr-Tf was prepared as previously reported (5). Three- to 5-week-old male *nu/nu* mice were obtained from Charles River. Mice were inoculated with 1×10^7 U87 MG or PC3 cells subcutaneously into one flank in a 1:1 mixture (v/v) of media and Matrigel (Corning). Tumors were palpable within 14 to 21 days after injection. The drugs were suspended in HPMT solution (0.5% w/v hydroxypropyl-methylcellulose dissolved in water plus 0.2% v/v Tween 80). Tumor-bearing mice were treated once daily via oral gavage with RAD001 (10 mg/kg/d), BEZ235 (25 mg/kg), doxorubicin (7.5 mg/kg), or INK-128 (1 mg/kg) for 4 days (2 days before the injection and 2 days following the radiotracer injection) except for the RAD001 where the mice were treated during 7 days (5 days before the injection and 2 days following the radiotracer injection).

Small-animal PET and biodistribution studies

Tumor-bearing mice ($n = 5$ per treatment arm) received about 300 μCi of ^{89}Zr-Tf in 100 μL volume intravenously using a custom mouse tail vein catheter with a 28-gauge needle and a 100- to 150-mm-long polyethylene microtubing (0.28 mm I.D. × 0.64 mm O.D., Scientific Commodities, Inc.). Approximately 32 μg of Tf at a specific activity of 0.4 mCi/nmol was administered per mouse. The mice were imaged on a dedicated small-animal PET/CT scanner (Inveon, Siemens Healthcare). Mice were imaged at 48 hours postinjection. Animals were scanned for 40 minutes for PET, and the CT acquisition was 10 minutes. The coregistration between PET and CT images was obtained using the rigid transformation matrix from the manufacturer-provided scanner calibration procedure since the geometry between PET and CT remained constant for each of PET/CT scans using the combined PET/CT scanner. Animals were anesthetized with gas isoflurane at 2% concentration mixed with medical grade oxygen. PET data were framed dynamically for the first 2 time points. The durations of the 0.5-hours PET data were: 10 × 10 seconds, 5 × 40 seconds, 1 × 300 seconds, and 5 × 600 seconds. The 3- to 5-hour PET data were also divided to two 1,800-second frames. The *in vivo* CT parameters were 120 projections of continuous rotations to cover 220° with an X-ray tube operated at 80 kVp, 0.5 mA, and 175 ms exposure time.

Manufacturer-provided ordered subsets expectation maximization (OS-EM) algorithm was used for PET reconstruction that resulted in $128 \times 128 \times 159$ matrices with a voxel size of $0.776 \times 0.776 \times 0.796$ mm^3. The CT image was created using a conebeam Feldkamp reconstruction algorithm (COBRA) provided by Exxim Computing Corporation. The matrix size of the reconstructed CT images was $512 \times 512 \times 662$ with an isotropic voxel size of $0.191 \times 0.191 \times 0.191$ mm^3. The photon attenuation correction was performed for PET reconstruction using the coregistered CT-based attenuation map to ensure the quantitative accuracy of the reconstructed PET data.

To evaluate the uptake of ^{89}Zr- Tf in human xenografts, biodistribution studies were conducted following imaging. Animals were euthanized by CO_2 asphyxiation after scans were completed. Sixteen tissues, including the tumor, were harvested immediately following sacrifice. The tissues were weighed and counted using a Wizard3 gamma counter (Perkin Elmer) to assess ^{89}Zr concentration. Calibration with known amounts of ^{89}Zr was performed to determine the amount of activity in each organ. This activity was then decay corrected, and the percentage of the injected dose per gram (%ID/g) of tissue was calculated and reported.

Statistical analysis

Data were analyzed using the unpaired, 2-tailed Student *t* test. Differences at the 99% confidence level ($P < 0.01$) were considered to be statistically significant.

Results

Activating genetic lesions within the PI3K/Akt/mTOR signaling axis enhance transferrin uptake into cancer cells *in vitro* and *in vivo*

We first studied the relationship between mTOR activity and Tf biology in a panel of human glioma and prostate cancer models, 2 diseases in which mTOR hyperactivation is prevalent and associated with poor clinical outcomes. We used shRNA to PTEN to generate 6 isogenic pairs of glioblastoma multiforme and prostate cancer cell lines and one immortalized prostate epithelial cell line (PrEC LHS, see Supplementary Fig. S1). Using radiolabeled Tf, we observed that PTEN knockdown sublines had 2- to 3-fold higher uptake of Tf compared with the respective isogenic wild-type subline (Fig. 1A). We next asked whether activating mutations in kinases within the signaling axis also upregulate Tf uptake into cells. To test this, HEK293 cells were transfected with a cDNA encoding p110α E545K, H1047R, wild-type, or empty vector (Supplementary Fig. S2). After 72 hours, about 50% increase in Tf uptake was observed in cells with p110α E545K or H1047R compared with wild-type or mock-transfected cells (Fig. 1B). Consistent with this finding, we also observed higher Tf uptake in HEK293 cells transfected with mTOR constructs harboring activating mutations (C1483F, E1799K, T1977R, S2215Y, R2505) compared with cells with overexpressed or endogenous levels of wild-type Mtor (ref. 6; Fig. 1C; Supplementary Fig. S3). Finally, we asked whether loss of the TSC1/2 complex resulted in higher Tf uptake *in vitro*. Tf uptake was shown to be higher in both NIH-3T3 cell lines with transient knockdown of TSC1 or 2 via siRNA and in MEFs with genetic deletion of TSC1 or 2 (Supplementary Figs. S4 and S5).

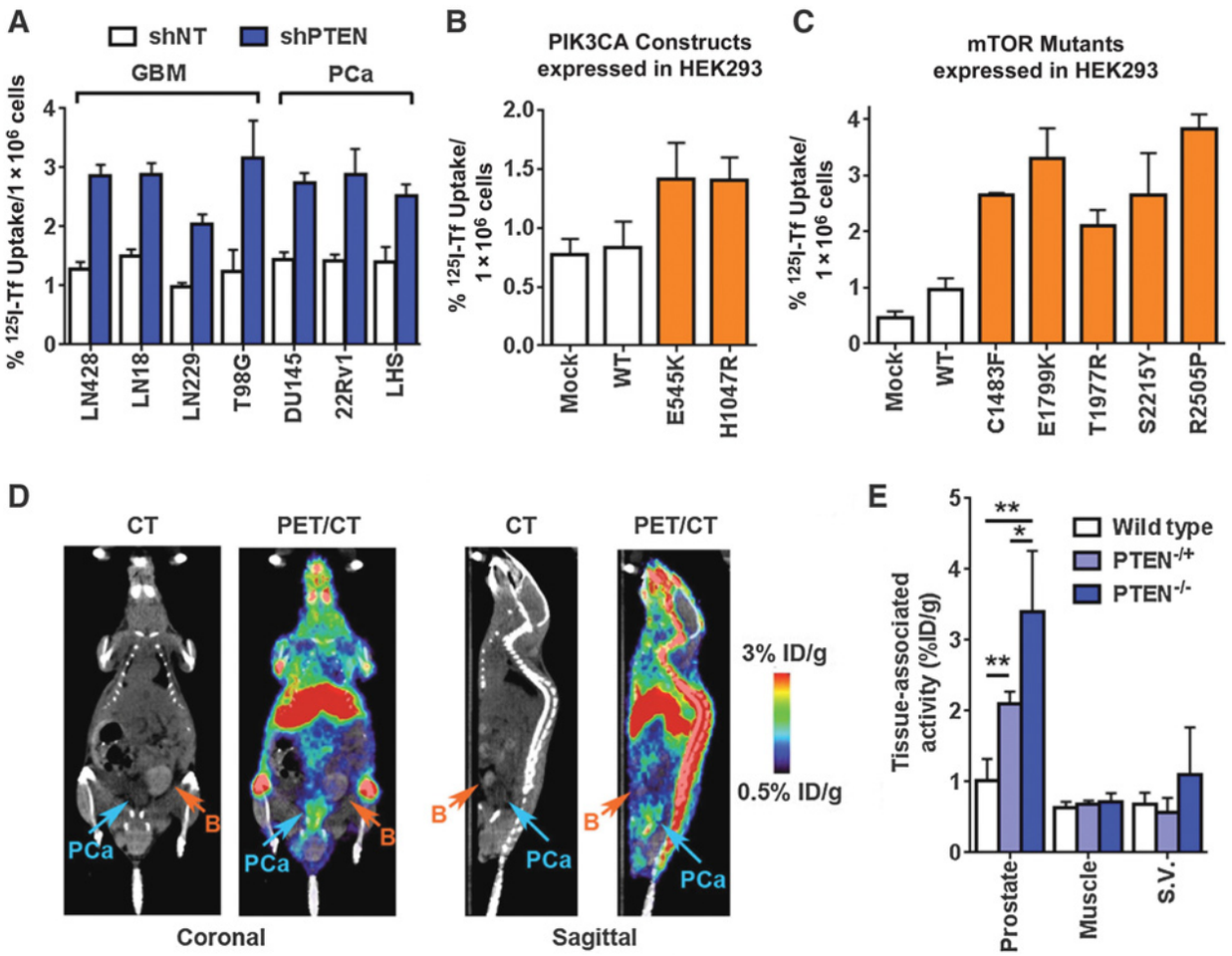

Figure 1.

Genetic lesions promoting PI3K pathway signaling increase transferrin uptake into glioblastoma multiforme and prostate cancer cells *in vitro* and *in vivo*. **A,** *In vitro* uptake data showing higher uptake of ^{125}I-Tf in PTEN-null glioblastoma multiforme and prostate cancer sublines. The data are expressed as a percentage of total activity to which the cells were exposed and normalized to cell number. Knockdown of PTEN was validated with rtPCR and immunoblot. All changes in transferrin uptake between the sublines were statistically significant ($P < 0.01$). **B,** *In vitro* uptake data showing higher uptake of ^{125}I-Tf in HEK293 cells transiently overexpressing mutant p110α compared with cells with endogenous or overexpressed p110α. Cells were transfected for 48 hours before conducting the uptake assay, and separate treatment arms were reserved to validate successful transfection via rtPCR. All changes in transferrin uptake between the cell lines transfected with mutant constructs were statistically significant compared with mock and untransfected, wild-type (WT) cells ($P < 0.01$). **C,** *In vitro* uptake data showing higher uptake of ^{125}I-Tf in HEK293 cells transiently overexpressing mutant mTOR compared with cells with endogenous or overexpressed wild-type mTOR. Cells were transfected for 48 hours before conducting the uptake assay, and separate treatment arms were reserved to validate successful transfection via rtPCR. All changes in transferrin uptake between the cell lines transfected with mutant constructs were statistically significant compared with mock and untransfected, wild-type cells ($P < 0.01$). **D,** Coronal and sagittal representation of the PET/CT data collected in a 10-month-old mouse with prostate-specific deletion of PTEN shows the uptake of ^{89}Zr-Tf in the prostate cancer tumor. The data were collected 48 hours postinjection, and the mouse was imaged for 60 minutes. The position of the bladder (**B**) is indicated with the orange arrow, whereas the position of the prostate cancer mass is indicated with a blue arrow. **E,** Biodistribution data for the prostate lobes and selected normal tissues show the incremental increase in ^{89}Zr-Tf uptake in prostate tissues as each PTEN allele is deleted. *, $P < 0.05$; **, $P < 0.001$.

We next tested whether genetically engineered mice harboring prostate-specific deletion of PTEN and mTOR activation have higher avidity for ^{89}Zr-Tf *in vivo*. We chose to study mice with ^{89}Zr-Tf as our previous work showed this radiotracer to have excellent pharmacokinetics *in vivo*, and this empowered images of spontaneous tumors in genetically engineered mice and orthotopic brain tumors (5, 7). A cohort of 10-month-old male mice with heterozygous or homozygous deletion of PTEN in the prostate (8), and age-matched wild type controls were injected with ^{89}Zr-Tf. Forty-eight hours postinjection, the animals were imaged using small-animal PET/CT. Virtually, no uptake was observed in the bladder, as expected, whereas an area of high radiotracer uptake was observed in a region posterior to the bladder (Fig. 1D). To confirm that this hotspot corresponded to ^{89}Zr-Tf uptake in prostate lobes with hyperactive mTORC1, the mice were euthanized, and components of the urogenital tract were plated on a petri dish and imaged in a PET/CT for 7 hours. After decay correcting the images, we observed visibly higher

radioactivity associated with the transgenic prostate lobes compared with the wild-type tissues and the nearby normal tissues (Supplementary Fig. S6). Measurement of the tissue-associated activity *ex vivo* showed statistically higher uptake of the radiotracer in the transgenic prostates compared with the wild-type lobes. Remarkably, we also observed statistically higher uptake of ^{89}Zr-Tf in the prostate lobes with homozygous PTEN deletion than in those with loss of one PTEN allele (Fig. 1E; Supplementary Fig. S7). This finding underscores the highly sensitive quantification of PI3K pathway signaling with ^{89}Zr-Tf. Moreover, because heterozygous mice have increased mTOR signaling but no overt disease phenotype, these data further highlight that ^{89}Zr-Tf uptake is pathway-driven and not just an indirect effect of cancer formation (8).

Inhibition of mTORC1 suppresses transferrin uptake *in vitro* and *in vivo*

We next asked whether Tf uptake is inhibited by targeted therapies in endogenously PTEN-null glioblastoma multiforme and prostate cancer cell lines. Tf uptake in 4 PTEN-null glioblastoma multiforme models (U138 MG, U251, U373 MG, and U87 MG) and 2 PTEN-null prostate cancer models (LNCaP-AR, PC3) was suppressed by the dual PI3K/mTOR inhibitor BEZ235 (Fig. 2A; Supplementary Fig. S8). Moreover, the inhibitory effects were time- and dose-dependent, pointing to specificity of this pharmacology (Supplementary Fig. S9). As our genetic data suggested that mTOR regulates Tf biology downstream of PI3K/Akt, we next tested whether the mTOR kinase inhibitor INK128 impacted Tf uptake. A clear time- and dose-dependent suppression of Tf uptake was observed (Fig. 2A; Supplementary Fig. S10). To distinguish which mTOR complex was responsible for regulating Tf uptake, we treated the cell lines with the mTORC1-specific allosteric site inhibitor RAD001. RAD001 inhibited Tf uptake to an extent equivalent to BEZ235 and INK128 (Fig. 2A; Supplementary Fig. S11). We next tested whether an antiproliferative drug that does not impact mTORC1 signaling affects Tf biology. The panel of PTEN-null cell lines was treated with bioactive doses of the genotoxic agent doxorubicin, and no change in Tf uptake or the levels of phosphorylated mTOR substrates was observed (Fig. 2A; Supplementary Fig. S12). Finally, we studied Tf regulation in HCT15 and T47D, 2 human cancer cell lines harboring p110α mutants E545K and H1047R, respectively. We observed similar trends in the data, as inhibition of mTORC1 suppressed Tf uptake in each model, and doxorubicin did not impact mTORC1 signaling or Tf uptake (Fig. 2B, see also Supplementary Figs. S13–S15).

These pharmacologic data suggest that mTORC1 regulates Tf biology, and to extend these data employing a genetic approach, we transiently transfected U87 MG cells with siRNAs targeting mTOR, the mTORC1 component Raptor (RPTOR), and the mTORC2 component proline-rich protein 5 (PRR5). While genetic ablation of mTOR and the mTORC1 component suppressed Tf uptake, disruption of an essential mTORC2 subunit did not affect Tf uptake (Fig. 2C; Supplementary Fig. S16).

To determine how mTORC1 regulates TFRC in our models, we studied TFRC mRNA and protein levels in U87 MG, LNCaP, and PC3 cells after 48-hour exposure to BEZ235, INK128, RAD001, or doxorubicin. The kinase inhibitors potently suppressed TFRC mRNA, and a reduction in TFRC protein level was evident by semiquantifying cell surface TFRC with a radiolabeled monoclonal antibody (Supplementary Fig. S17). No effect on TFRC mRNA or protein was observed in any of the cell lines after treatment with doxorubicin. We next asked whether genetic ablation of mTORC1 suppressed TFRC transcription. Consistent with the pharmacologic data, siRNA knockdown of mTOR and RAPTOR in U87MG cells repressed TFRC mRNA and protein, whereas knockdown of PRR5 did not change TFRC mRNA or protein levels (Supplementary Fig. S18).

Not all drug-induced biologic changes are sufficiently large or durable to be quantified with PET; therefore, we next asked whether pharmacologic inhibition of mTORC1 could be measured with ^{89}Zr-Tf PET *in vivo*. Male *nu/nu* mice bearing subcutaneous U87 MG, LNCaP-AR, or PC3 tumors were treated once daily via oral gavage with vehicle, BEZ235, INK128, or doxorubicin for 2 days—RAD001 was administered once daily for 5 days—and injected with ^{89}Zr-Tf. Two days after the injection of ^{89}Zr-Tf, the mice were imaged with PET/CT and euthanized (drug treatment continued after injection of ^{89}Zr-Tf). In U87MG tumors, mTORC1 inhibitors reduced ^{89}Zr-Tf uptake by about 75% (Fig. 2D and E, see Supplementary Fig. S19). As expected, a bioactive dose of doxorubicin did not impact mTORC1 signaling and ^{89}Zr-Tf uptake in the tumor. Region-of-interest analysis of the U87 MG tumors corroborated the biodistribution data (Supplementary Fig. S20). We observed a similar trend in the data generated with mice bearing LNCaP-AR and PC3 tumors (Fig. 2D and E, see Supplementary Fig. S21 for the LNCaP-AR biodistribution data and Supplementary Fig. S22 for the PC3 biodistribution data).

^{89}Zr-transferrin PET can measure the inducible upregulation of mTORC1 as a mechanism of resistance to standard-of-care antiandrogen therapy

Because acquired resistance to targeted therapies is so pervasive, defining actionable resistance mechanisms is one of the most important frontiers in translational cancer research. Preclinical studies show that multiple resistance mechanisms often arise from a single therapy, and understanding which is active in a given patient would be ideal for determining the next course of treatment or eligibility for a clinical trial. Because the "druggable" molecular drivers of the uptake machinery for common, human ready radiotracers (e.g., ^{18}F-FDG, ^{11}C-acetate, ^{11}C-choline) are poorly understood or unknown, PET is not currently applied to study the mechanisms underpinning treatment-resistant cancer. Developing ^{89}Zr-Tf provided the opportunity to conduct the first study to determine whether PET can be used instead of invasive tissue sampling to characterize the biology of treatment-resistant cancer.

Castration-resistant prostate cancer (CRPC) acquires resistance to antiandrogens like enzalutamide and ARN-509 within 16 months through a variety of mechanisms. The preclinical model LNCaP-AR was recently used to discover 3 clinically relevant and actionable mechanisms: escape from therapy due to the transactivation of mTORC1 (9–11), point mutation in the androgen receptor to convert antagonist to agonist (12, 13), and overexpression of the glucocorticoid receptor to restore AR signaling (14). The molecular diversity of these resistance mechanisms emerging from this clinically validated model of CRPC provided the cellular background to test whether ^{89}Zr-Tf PET can distinguish resistant cells harboring hyperactive mTORC1.

We first tested whether pharmacologic changes in AR signaling would impact Tf biology in an mTORC1-dependent fashion *in vitro*. Treatment of LNCaP-AR cells with a bioactive dose of the

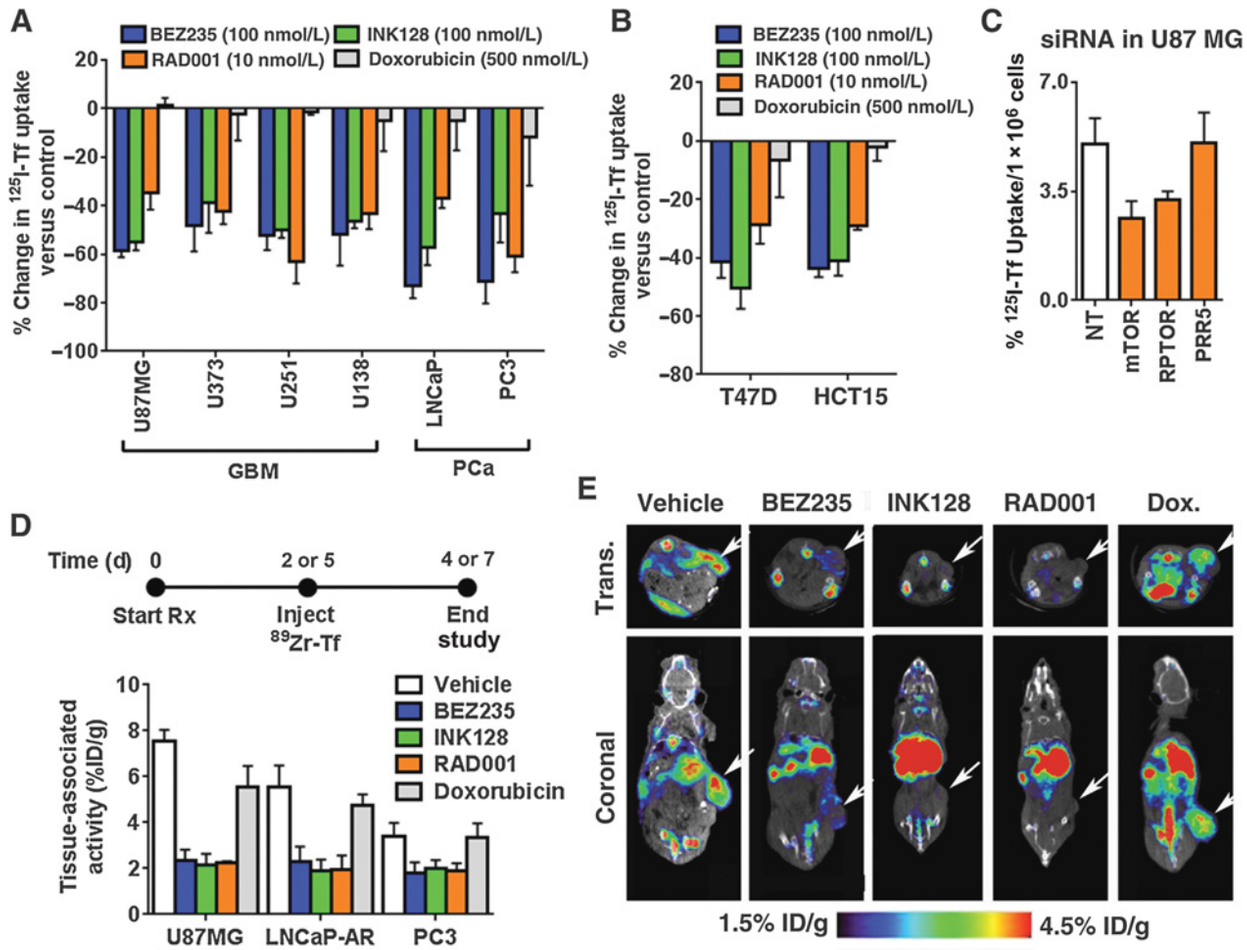

Figure 2.

Pharmacologic and genetic inhibition of mTORC1 suppresses Tf uptake in glioblastoma multiforme and prostate cancer models *in vitro* and *in vivo*. **A,** *In vitro* uptake data showing that BEZ235 (100 nmol/L), INK128 (100 nmol/L), and RAD001 (10 nmol/L) suppresses transferrin uptake in endogenously PTEN-null glioblastoma multiforme and prostate cancer cell lines. No effect was observed for a bioactive dose doxorubicin (500 nmol/L) that reduces cell number in an mTOR-independent fashion. Target inhibition was confirmed by immunoblot. All uptake data were normalized to cell number at the start of the incubation with ^{125}I-Tf. All changes in transferrin uptake due to kinase inhibitor treatments were statistically significant compared with vehicle- and doxorubicin-treated cells ($P < 0.01$). **B,** *In vitro* uptake data showing that BEZ235 (100 nmol/L), INK128 (100 nmol/L), and RAD001 (10 nmol/L) suppresses transferrin uptake in T47D and HCT15, 2 cell lines harboring activating mutations in PIK3CA. No effect was observed for a bioactive dose doxorubicin (500 nmol/L). Target inhibition was confirmed by immunoblot. All uptake data were normalized to cell number at the start of the incubation with ^{125}I-Tf. All changes in transferrin uptake due to kinase inhibitor treatments were statistically significant compared with vehicle- and doxorubicin-treated cells ($P < 0.01$). **C,** *In vitro* uptake data showing that siRNAs targeting mTOR and the mTORC1 component RPTOR suppress transferrin uptake, whereas ablation of the mTORC2 component PRR5 did not impact transferrin uptake. HEK293 cells were transfected with siRNAs and studied 48 hours postinjection. Gene silencing was confirmed with siRNA. All uptake data were normalized to cell number at the start of the incubation with ^{125}I-Tf. All changes in transferrin uptake due to mTORC1 silencing were statistically significant compared with mock and PRR5 siRNA–transfected cells. **D,** Biodistribution data for U87 MG and PC3 subcutaneous tumors after short-term treatment with vehicle, BEZ235 (25 mg/kg), INK128 (1 mg/kg), RAD001 (10 mg/kg), and doxorubicin (7.5 mg/kg). Large and statistically significant ($P < 0.01$) changes in radiotracer uptake were only observed in the tumors exposed to mTORC1 inhibitors. No statistically significant change in tumor volume was observed after this short-treatment interval. **E,** Representative coronal and transverse PET slices showing the magnitude of radiotracer uptake in mice bearing U87 MG tumors. The subcutaneous tumors are located on the right flank. ROI analysis also distinguished the differences in radiotracer uptake among the treatment arms, with mTORC1 inhibition suppressing ^{89}Zr-Tf uptake, and no change noted with doxorubicin.

antiandrogen ARN-509 dramatically upregulated TFRC mRNA and Tf uptake after a 48-hour exposure (Fig. 3A; Supplementary Fig. S23). Moreover, cotreatment of ARN-509 and RAD001 suppressed the induction of TFRC mRNA and Tf uptake, showing the ARN-509 induction of Tf uptake requires mTORC1, as expected. Finally, RAD001 suppressed TFRC mRNA and Tf uptake to a degree equivalent to AR agonism by dihydrotestosterone.

We next tested whether this effect could be quantified with ^{89}Zr-Tf PET *in vivo*. LNCaP-AR tumors were established subcutaneously in intact mice. A visually obvious induction of ^{89}Zr-Tf was observed by PET in the tumors of mice treated with ARN-509 for 4 days compared with mice receiving vehicle or ARN-509 with RAD001 (Fig. 3B). Biodistribution studies showed approximately 2-fold higher activity in the tumors treated with ARN-509

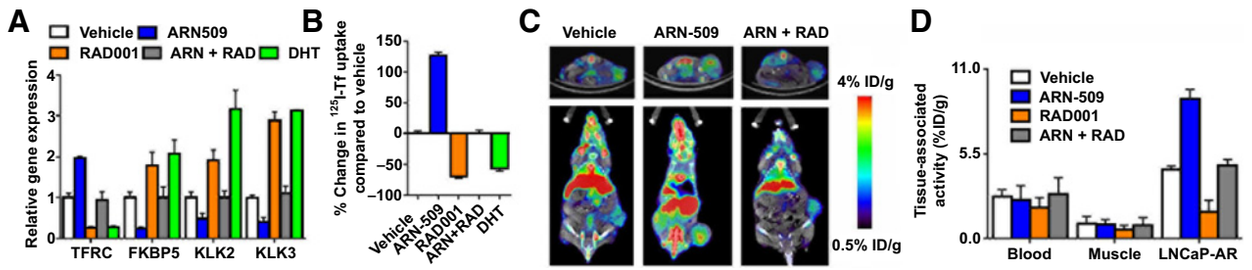

Figure 3.

Transactivation of mTORC1 by androgen receptor inhibition can be measured with radiolabeled Tf *in vitro* and *in vivo*. **A,** Real-time PCR data showing the relative changes in TFRC and androgen receptor target genes in response to stimulation or inhibition of the androgen receptor. Treatment with the antiandrogen ARN-509 (10 μmol/L) for 72 hours results in upregulation of TFRC mRNA and effect that is reversed by cotreatment with RAD001 (10 nmol/L). Conversely, treatment with dihydrotestosterone (DHT; 10 nmol/L) suppresses TFRC mRNA levels. RAD001 treatment reduced TFRC mRNA, as expected. Androgen receptor target genes were stimulated or repressed in a manner consistent with what was previously reported. All changes in mRNA levels due to AR stimulation or repression were statistically significant compared with vehicle and combined ARN/RAD001 therapy ($P < 0.01$). **B,** *In vitro* uptake data with ^{125}I-Tf show that ARN-509 upregulates Tf uptake in an mTORC1-dependent fashion, as predicted by the rtPCR data. Data were collected after 72 hours of incubation with drug. All changes in transferrin uptake due to mTORC1 stimulation or repression were statistically significant compared with vehicle and combined ARN/RAD001 therapy ($P < 0.01$). **C,** Representative coronal and transverse PET/CT images showing the tumor uptake of ^{89}Zr-Tf in mice bearing LNCaP-AR tumors. Separate treatment arms received ARN-509 (30 mg/kg), RAD001 (10 mg/kg), or both therapies via gavage for 2 days prior to injection with ^{89}Zr-Tf. The radiotracer distributed for 48 hours before collecting the PET/CT data. The subcutaneous tumor is located on the right flank. **D,** Biodistribution data showing the relative uptake of ^{89}Zr-Tf in the tumor tissue, muscle, and blood. The pattern of radiotracer uptake in the tumor is consistent with the *in vitro* data and the relative intensity of the PET images. All changes in transferrin uptake in the tumor due to mTORC1 stimulation or repression were statistically significant compared with vehicle and combined ARN/RAD001 therapy ($P < 0.01$).

compared with vehicle or ARN-509 with RAD001 (Fig. 3C and D, see also Supplementary Fig. S24). Collectively, these studies show that ^{89}Zr-Tf can detect cells within a tumor that evade antiandrogen therapy by upregulating mTORC1.

Discussion

In this report, we disclose a new nuclear imaging probe to noninvasively and globally measure the signaling dynamics of mTORC1 in higher organisms. Proof-of-concept studies were conducted in cell and animal models of glioblastoma multiforme and prostate cancer, 2 cancers in which high mTOR signaling is prevalent but not uniform, and also not predictable with the current repertoire of noninvasive or minimally invasive diagnostics. We show that mTORC1 (and not mTORC2) activation results in higher cellular uptake of Tf *in vitro* and *in vivo*, making cells with aberrant mTORC1 activity more visible by PET than those with quiescent signaling. Importantly, ^{89}Zr-Tf PET detects aberrant mTORC1 signaling in small foci of normal prostate cells prior to their transformation to neoplastic cells or adenocarcinoma, showing that cellular uptake of ^{89}Zr-Tf is not an emergent feature of hyperproliferative cells. We also show that ^{89}Zr-Tf can be exploited to use PET for the first time to characterize the intracellular mechanism by which a cancer cell acquires resistance to targeted therapy. All of these preclinical studies provide the foundation for impactful first in human study, and we are currently preparing an IND submission.

The observation that ^{89}Zr-Tf measures mTORC1 signaling in normal tissues gives could give rise to research and clinical applications for PET beyond what is currently considered. As very little is understood about the mechanism by which mTORC1 is activated in adult mice to cause spontaneous tumorigenesis, one implication for preclinical research is that ^{89}Zr-Tf can be applied to isolate and further study individual cells harboring hyperactive mTORC1 *ex vivo*. Clinically, ^{89}Zr-Tf could be applied in an analogous fashion to screen for benign masses that are transitioning to malignancy due to mTOR hyperactivation. This is a major unmet need for mTOR-driven inherited disorders like tuberous sclerosis complex or neurofibromatosis that result in multiple benign masses which progress unpredictably to incurable malignancies during childhood or adolescence (15, 16).

The finding showing that ^{89}Zr-Tf can detect the transactivation of mTORC1 *in vivo* by an antiandrogen also provides an instructive example as to how developing a radiotracer responsive to an intracellular oncogene could expand the role for PET in clinical practice. The example presented in models of CRPC is especially provocative, as CRPC is highly common, notoriously challenging to biopsy, and molecularly heterogeneous resistance mechanisms have already been documented in small patient cohorts with enzalutamide- or ARN-509–resistant disease. Our data argue for an immediate large-scale human study with ^{89}Zr-Tf to define the frequency of resistance due to this mechanism, especially considering it is actionable with human ready therapies.

Another exciting outcome of this study is that ^{89}Zr-Tf may finally allow the scientific community to systematically measure the pharmacodynamics of targeted therapies addressing kinases in the PI3K signaling pathway in larger patient cohorts over multiple centers. This is important, as prior lessons from clinical trials clearly show that complete and durable target coverage is necessary for targeted therapies to induce clinical responses. For example, a phase I dose-escalation study in a small panel of patients with glioblastoma showed that phospho-S6 suppression by rapamycin was required to observe reduced Ki-67 staining (17). More recently, post-vemurafenib biopsies showed that more than 85% suppression of phospho-ERK was needed for clinical responses in BRAF V600E melanoma (18). Therefore, the finding that ^{89}Zr-Tf can measure pharmacologically inhibition of mTORC1 could position the field to conduct the first large-scale studies to correlate target blockade with clinical responses in any cancer, regardless of the opportunity for biopsy. Finally,

enthusiasm for anti-mTORC1 therapies remains high, as there are more than 300 active trials in the United States studying the antitumor effects of RAD001 (www.clinicaltrials.gov), whereas isoform-specific inhibitors of p110 have also showed exciting preclinical and clinical activities (19).

To our knowledge, ^{89}Zr-Tf is the first nuclear imaging tool intentionally developed to measure mTORC1 activity in normal and cancer tissues. While the uptake of radiolabeled glucose molecules is activated by mTOR in normal insulin-responsive tissues like brown fat and muscle (20, 21), the connection between mTOR and glucose uptake in cancer is far less clear. For instance, ^{18}F-FDG uptake in breast cancer and colorectal cancer models is not mTORC1-driven (22, 23). Moreover, although CRPC is almost uniformly PTEN-null, this disease is not avid for ^{18}F-FDG, suggesting that mTORC1 activation does not inherently result in elevated glucose uptake in cancer (24). In contrast, we recently showed that CRPC is broadly avid for radiolabeled Tf (25). A study of 8 patients at UCSF showed that 71 of 96 detectable metastases were avid for ^{68}Ga-Tf (formed in situ after the administration of ^{68}Ga-citrate intravenously). Importantly, about 25% of lesions were not avid for ^{68}Ga-Tf, suggesting that tumor localization is due to receptor binding, and not vascular effects as has been suggested previously (26). Finally, these imaging data are consistent with a heterogeneous molecular landscape known to be enriched in hyperactive mTORC1 and bode well for the pending first-in-man study with ^{89}Zr-Tf.

We are also optimistic that ^{89}Zr-Tf will be a powerful complement to magnetic resonance (MR)-based biomarkers like 1-^{13}C-pyruvate (27). We are particularly confident that ^{89}Zr-Tf will excel in detecting small disease foci in the metastatic setting where MR-based probes are challenging to implement. Moreover, with the recent commercialization of hybrid clinical PET/MR scanners, multiple dimensions of PI3K pathway signaling may be evaluable within a single examination, which would allow for the study of cancer metabolism in humans with an unprecedented degree of complexity.

To our knowledge, this is the first effort to mine the biology downstream of mTOR to identify a nuclear imaging biomarker for this very important signaling molecule. Our success showing that the intracellular biochemistry of mTORC1, itself currently unamenable to targeting with PET, can be imaged by targeting a downstream cell surface receptor gives us optimism that this approach may be applied to many more central oncogenes currently refractory to nuclear imaging.

Disclosure of Potential Conflicts of Interest

M.J. Evans is a paid consultant for ORIC Pharmaceuticals and reports receiving commercial research grants from General Electric. No potential conflicts of interest were disclosed by the other authors.

Disclaimer

The content is solely the responsibility of the authors and does not necessarily represent the official views of the NIH.

Authors' Contributions

Conception and design: C. Truillet, J.T. Cunningham, D. Ruggero, J.S. Lewis, M.J. Evans

Development of methodology: J.S. Lewis

Acquisition of data (provided animals, acquired and managed patients, provided facilities, etc.): C. Truillet, J.T. Cunningham, M.F.L. Parker, L.T. Huynh

Analysis and interpretation of data (e.g., statistical analysis, biostatistics, computational analysis): C. Truillet, J.T. Cunningham, D. Ruggero, J.S. Lewis, M.J. Evans

Writing, review, and/or revision of the manuscript: C. Truillet, J.T. Cunningham, D. Ruggero, J.S. Lewis, M.J. Evans

Administrative, technical, or material support (i.e., reporting or organizing data, constructing databases): C.S. Conn, J.S. Lewis

Study supervision: J.S. Lewis, M.J. Evans

Acknowledgments

The authors acknowledge Dr. Youngho Seo and Sergio Wong of the Small Animal Imaging Core at UCSF for technical assistance.

Grant Support

C. Truillet was supported by a postdoctoral fellowship from the Department of Defense Prostate Cancer Research Program (PC151060). J.T. Cunningham, C.S. Conn, and D. Ruggero were supported, in part, by the National Cancer Institute (R01CA154916). M.J. Evans was supported by the 2013 David H. Koch Young Investigator Award from the Prostate Cancer Foundation, the NIH (R00CA172695, R01CA17661), a Department of Defense Idea Development Award (PC140107), the UCSF Academic Senate, and GE Healthcare. Research from UCSF reported in this publication was supported in part by the National Cancer Institute of the NIH under Award Number P30CA082103. The work at MSKCC is supported in part by NIH Cancer Center Support Grant P30CA008748.

The costs of publication of this article were defrayed in part by the payment of page charges. This article must therefore be hereby marked *advertisement* in accordance with 18 U.S.C. Section 1734 solely to indicate this fact.

Received October 5, 2016; revised December 9, 2016; accepted December 9, 2016; published OnlineFirst December 22, 2016.

References

1. Laplante M, Sabatini DM. mTOR signaling in growth control and disease. Cell 2012;149:274–93.
2. Evans MJ.Measuring oncogenic signaling pathways in cancer with PET: an emerging paradigm from studies in castration-resistant prostate cancer. Cancer Discov 2012;2:985–94.
3. O'Donnell KA, Yu D, Zeller KI, Kim JW, Racke F, Thomas-Tikhonenko A, Dang CV. Activation of transferrin receptor 1 by c-Myc enhances cellular proliferation and tumorigenesis. Mol Cell Biol 2006;26:2373–86.
4. Bianchi L, Tacchini L, Cairo G. HIF-1-mediated activation of transferrin receptor gene transcription by iron chelation. Nucleic Acids Res 1999; 27:4223–7.
5. Holland JP, Evans MJ, Rice SL, Wongvipat J, Sawyers CL, Lewis JS. Annotating MYC status with 89Zr-transferrin imaging. Nat Med 2012;18:1586–91.
6. Grabiner BC, Nardi V, Birsoy K, Possemato R, Shen K, Sinha S, et al. A diverse array of cancer-associated MTOR mutations are hyperactivating and can predict rapamycin sensitivity. Cancer Discov 2014;4: 554–63.
7. Evans MJ, Holland JP, Rice SL, Doran MG, Cheal SM, Campos C, et al. Imaging tumor burden in the brain with 89Zr-transferrin. J Nucl Med 2013;54:90–5.
8. Wang S, Gao J, Lei Q, Rozengurt N, Pritchard C, Jiao J, et al. Prostate-specific deletion of the murine Pten tumor suppressor gene leads to metastatic prostate cancer. Cancer Cell 2003;4:209–21.
9. Carver BS, Chapinski C, Wongvipat J, Hieronymus H, Chen Y, Chandarlapaty S, et al. Reciprocal feedback regulation of PI3K and androgen receptor signaling in PTEN-deficient prostate cancer. Cancer Cell 2011;19:575–86.
10. Squillace RM, Miller D, Wardwell SD, Wang F, Clackson T, Rivera VM. Synergistic activity of the mTOR inhibitor ridaforolimus and the antiandrogen bicalutamide in prostate cancer models. Int J Oncol 2012;41:425–32.

11. Nakabayashi M, Werner L, Courtney KD, Buckle G, Oh WK, Bubley GJ, et al. Phase II trial of RAD001 and bicalutamide for castration-resistant prostate cancer. BJU Int 2012;110:1729–35.
12. Balbas MD, Evans MJ, Hosfield DJ, Wongvipat J, Arora VK, Watson PA, et al. Overcoming mutation-based resistance to antiandrogens with rational drug design. eLife 2013;2:e00499.
13. Joseph JD, Lu N, Qian J, Sensintaffar J, Shao G, Brigham D, et al. A clinically relevant androgen receptor mutation confers resistance to second-generation antiandrogens enzalutamide and ARN-509. Cancer Discov 2013;3:1020–9.
14. Arora VK, Schenkein E, Murali R, Subudhi SK, Wongvipat J, Balbas MD, et al. Glucocorticoid receptor confers resistance to antiandrogens by bypassing androgen receptor blockade. Cell 2013;155:1309–22.
15. Luat AF, Makki M, Chugani HT. Neuroimaging in tuberous sclerosis complex. Curr Opin Neurol 2007;20:142–50.
16. Salamon J, Mautner VF, Adam G, Derlin T. Multimodal imaging in neurofibromatosis type 1-associated nerve sheath tumors. RoFo 2015;187:1084–92.
17. Cloughesy TF, Yoshimoto K, Nghiemphu P, Brown K, Dang J, Zhu S, et al. Antitumor activity of rapamycin in a Phase I trial for patients with recurrent PTEN-deficient glioblastoma. PLoS Med 2008;5:e8.
18. Bollag G, Tsai J, Zhang J, Zhang C, Ibrahim P, Nolop K, et al. Vemurafenib: the first drug approved for BRAF-mutant cancer. Nat Rev 2012;11:873–86.
19. Yang Q, Modi P, Newcomb T, Queva C, Gandhi V. Idelalisib: first-in-class PI3K delta inhibitor for the treatment of chronic lymphocytic leukemia, small lymphocytic leukemia, and follicular lymphoma. Clin Cancer Res 2015;21:1537–42.
20. Kaira K, Serizawa M, Koh Y, Takahashi T, Yamaguchi A, Hanaoka H, et al. Biological significance of 18F-FDG uptake on PET in patients with non-small-cell lung cancer. Lung Cancer 2014;83:197–204.
21. Thomas GV, Tran C, Mellinghoff IK, Welsbie DS, Chan E, Fueger B, et al. Hypoxia-inducible factor determines sensitivity to inhibitors of mTOR in kidney cancer. Nat Med 2006;12:122–7.
22. Nguyen QD, Perumal M, Waldman TA, Aboagye EO. Glucose metabolism measured by [(1)(8)F]fluorodeoxyglucose positron emission tomography is independent of PTEN/AKT status in human colon carcinoma cells. Translat Oncol 2011;4:241–8.
23. Palaskas N, Larson SM, Schultz N, Komisopoulou E, Wong J, Rohle D, et al. 18F-fluorodeoxy-glucose positron emission tomography marks MYC-over-expressing human basal-like breast cancers. Cancer Res 2011;71:5164–74.
24. Jadvar H. Prostate cancer: PET with 18F-FDG, 18F- or 11C-acetate, and 18F- or 11C-choline. J Nucl Med 2011;52:81–9.
25. Behr SC, Aggarwal R, Seo Y, Aparici CM, Chang E, Gao KT, et al. A feasibility study showing [Ga]Citrate PET detects prostate cancer. Mol Imaging Biol 2016;18:946–51.
26. Mintun MA, Dennis DR, Welch MJ, Mathias CJ, Schuster DP. Measurements of pulmonary vascular permeability with PET and gallium-68 transferrin. J Nucl Med 1987;28:1704–16.
27. Nelson SJ, Kurhanewicz J, Vigneron DB, Larson PEZ, Harzstark AL, Ferrone M, et al. Metabolic imaging of patients with prostate cancer using hyperpolarized [1-(1)(3)C]pyruvate. Sci Translat Med 2013;5:198ra108.